Research Square

Preprints are preliminary reports that have not undergone peer review.
They should not be considered conclusive, used to inform clinical practice,
or referenced by the media as validated information.

A Piezoelectric-Signal-Based Joint Angle Prediction Model for Wearable Systems

Zongyuan Li
Zhengzhou University
Yanzhi Tang
Zhengzhou University
Kexin Su
Zhengzhou University
Zhimin Chen
Zhengzhou University
Suyan Chen
Zhengzhou University
Ruijuan Wang
r.jwang@zzu.edu.cn

Zhengzhou University

Article

Keywords:

Posted Date: November 16th, 2026

DOI: https://doi.org/10.21203/rs.3.rs-11452998/v1

License: This work is licensed under a Creative Commons Attribution 4.0 International License.
Read Full License

Additional Declarations: No competing interests reported.

A Piezoelectric-Signal-Based Joint Angle Prediction Model for Wearable Systems

Zongyuan Li[1], Yanzhi Tang[2], Kexin Su[1], Zhimin Chen[2], Suyan Chen[3], and Ruijuan Wang[1,*]

[1]School of Cyber Science and Engineering, Zhengzhou University, Zhengzhou, China
[2]School of Materials Science and Engineering, Zhengzhou University, Zhengzhou, China
[3]School of Nursing and Health, Zhengzhou University, Zhengzhou, China
[*]Correspondence and requests for materials should be addressed to R.W. (rjwang@zzu.edu.cn).

ABSTRACT

Joint angle prediction is relevant to wearable motion monitoring, human–machine interaction, exoskeleton control, and rehabilitation assessment. Flexible piezoelectric sensors offer mechanical compliance, low cost, and fast dynamic response, but their voltage outputs are affected by random noise, sensor–skin contact, and local deformation fluctuations. These factors lead to low signal-to-noise ratio, nonstationarity, and nonlinear signal–angle relationships. This study proposes an NAE-Transformer (Noise-Aware Efficient Transformer) for joint angle prediction using a single flexible piezoelectric sensor. The model forms a dual-representation input by combining a Kalman-smoothed trend signal with a sliding-window noise-envelope feature, and uses a hybrid sparse attention encoder to capture temporal dependencies. Experiments were performed on a custom-built flexible piezoelectric sensor dataset, with a passive mechanical arm angle sensor used as the reference standard. Compared with LSTM (long short-term memory), Transformer, Informer, and their Kalman-filter-enhanced variants, NAE-Transformer obtained lower prediction error and higher goodness of fit. The results indicate that joint use of trend smoothing, local fluctuation representation, and hybrid sparse attention can improve piezoelectric-signal-based joint angle estimation under noisy and nonstationary sensing conditions.

Introduction

Joint angle prediction is a central task in wearable motion monitoring, rehabilitation-assisted training, human–machine interaction, and exoskeleton control. Accurate estimation of joint motion states supports objective rehabilitation assessment, timely exoskeleton response, and stable human–machine coordination[1–3]. Existing wearable approaches commonly rely on IMUs (inertial measurement units), sEMG (surface electromyography), or flexible sensors. IMU-based methods are affected by drift, magnetic interference, and mounting errors[4–9], whereas sEMG signals are sensitive to electrode placement, skin impedance, muscle fatigue, and inter-subject variability[1,10]. Flexible sensors provide a compliant and low-cost route for monitoring body-surface deformation[11,12].

Flexible piezoelectric sensors have been investigated for wearable motion sensing because of their structural compliance, self-powered response, fast dynamics, and low system cost[13–17]. More broadly, artificial-intelligence-assisted wearable flexible sensors are increasingly used for motion monitoring and temporal signal interpretation[18]. In practical use, however, piezoelectric signals are jointly influenced by muscle deformation, sensor–skin contact, motion speed, and environmental noise. They therefore often exhibit low signal-to-noise ratio, nonstationarity, and local fluctuations. Joint angle prediction from flexible piezoelectric signals is consequently a nonlinear temporal mapping problem.

Deep learning models can learn temporal features from sensor sequences and have been used for activity recognition, motion estimation, and joint angle prediction[19–23]. Recurrent models such as LSTM (long short-term memory) and GRU (gated recurrent unit) have been applied to joint angle estimation[24,25], although their sequential computation can limit long-range dependency modeling. Transformer-based models provide a direct mechanism for temporal dependency modeling through self-attention[26–29]; however, standard attention can introduce redundant computation and may be sensitive to local abnormal fluctuations under noisy sensing conditions. Kalman filtering improves signal smoothness[30–32], but relying only on a filtered signal may attenuate local dynamic information that remains useful for angle prediction.

This study proposes an NAE-Transformer (Noise-Aware Efficient Transformer) for joint angle prediction using a single flexible piezoelectric sensor. The model combines a Kalman-smoothed trend signal with a sliding-window noise envelope to form a dual-representation input, and uses a hybrid sparse attention encoder for temporal dependency modeling. The study makes three contributions: (1) a single-sensor dual-representation strategy for noisy and nonstationary piezoelectric signals; (2) a hybrid attention encoder that combines standard self-attention with ProbSparse attention; and (3) experimental validation using a custom-fabricated flexible piezoelectric sensor system, including quantitative comparison, ablation analysis, and three-dimensional motion reconstruction.

Problem Formulation and Signal Preprocessing

Joint Angle Prediction Problem

This study predicts absolute and relative joint angles from a single piezoelectric voltage sequence. Let $\mathbf{v} = \{v_1, v_2, \ldots, v_N\}$ denote the raw voltage sequence and $\theta = \{\theta_1, \theta_2, \ldots, \theta_N\}$ denote the corresponding reference angle sequence. The prediction targets are defined as

$$y_t^{\text{abs}} = \theta_t, \qquad y_t^{\text{rel}} = \theta_{t+1} - \theta_t. \tag{1}$$

A sliding window with length $T = 20$ is used to construct each sample,

$$X^{(i)} = [X_i, X_{i+1}, \ldots, X_{i+T-1}] \in \mathbb{R}^{T\times 2}, \tag{2}$$

where X_t is the dual-representation vector at time step t.

Kalman-Based Signal Smoothing

Kalman filtering is used to suppress high-frequency random noise while preserving the overall deformation trend of the piezoelectric signal. The state and observation equations are

$$x_k = Ax_{k-1} + Bu_k + w_k, \qquad z_k = Hx_k + v_k, \tag{3}$$

where x_k and z_k denote the system state and observation, respectively, and w_k and v_k denote process and observation noise. The process noise covariance and observation noise covariance are set to $Q = 10^{-5}$ and $R = 10^{-2}$, respectively.

Sliding-Window Noise Envelope Extraction

Local fluctuations may reflect muscle deformation, contact variation, and motion speed in addition to random noise. Therefore, the sliding-window standard deviation is extracted from the raw signal as a noise-envelope feature. The local neighborhood and its standard deviation are defined as

$$\Omega_t = \{i \mid \max(1, t - \lfloor W/2 \rfloor) \le i < \min(N, t + \lfloor W/2 \rfloor)\}, \tag{4}$$

$$\mu_t = \frac{1}{|\Omega_t|}\sum_{i\in\Omega_t} v_i, \qquad v_t^{\text{std}} = \sqrt{\frac{1}{|\Omega_t|}\sum_{i\in\Omega_t}(v_i - \mu_t)^2}. \tag{5}$$

The sliding window length is set to $W = 20$.

Dual-Representation Input Construction

The final input at time step t is constructed by combining the Kalman-filtered signal and the noise-envelope feature

$$X_t = [v_t^{\text{KF}}, v_t^{\text{std}}], \qquad X^{(i)} \in \mathbb{R}^{20\times 2}. \tag{6}$$

Fig. 1 shows the dual-representation input construction. The Kalman-filtered signal represents the overall trend, whereas the sliding-window standard deviation represents local fluctuation intensity.

Proposed NAE-Transformer Framework

Overall Architecture

The proposed NAE-Transformer uses the dual-representation sequence as input, maps it to a high-dimensional temporal representation, models temporal dependencies with a hybrid sparse attention encoder, and predicts absolute and relative joint angles through two regression heads. The overall architecture of the proposed framework is shown in Fig. 2. Compared with models based only on a filtered signal, the proposed model retains local fluctuation information. Compared with a standard Transformer encoder, it introduces ProbSparse attention in the higher encoder layer to reduce redundant attention interactions and emphasize informative time steps.

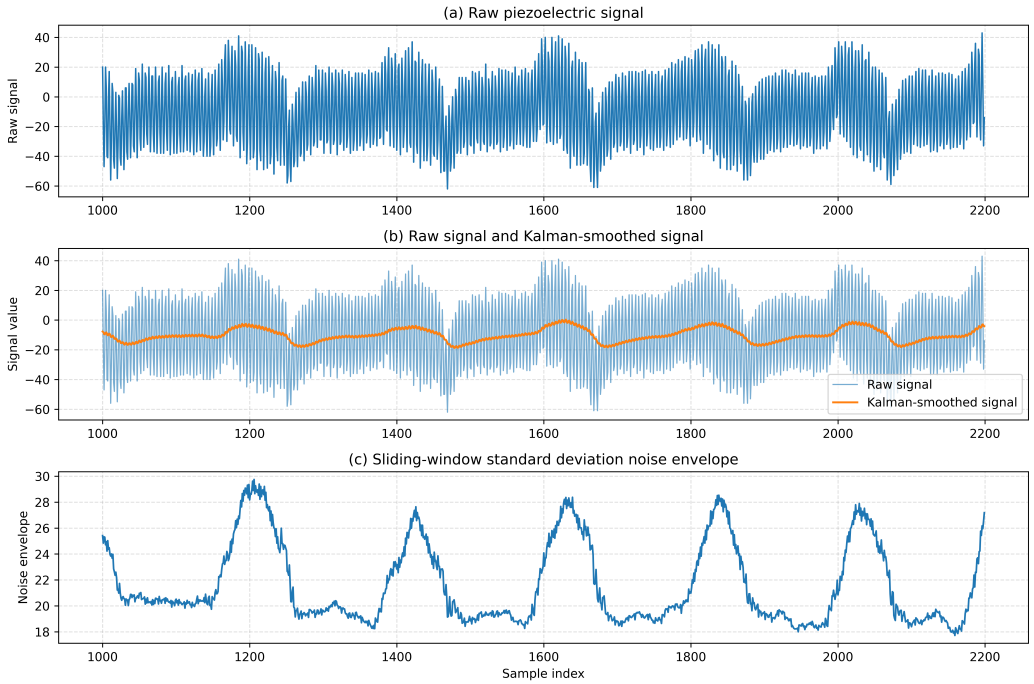


Figure 1. Piezoelectric signal preprocessing and dual-representation input construction: (a) raw piezoelectric signal, (b) comparison between the raw signal and the Kalman-smoothed signal, and (c) noise envelope extracted using the sliding-window standard deviation.

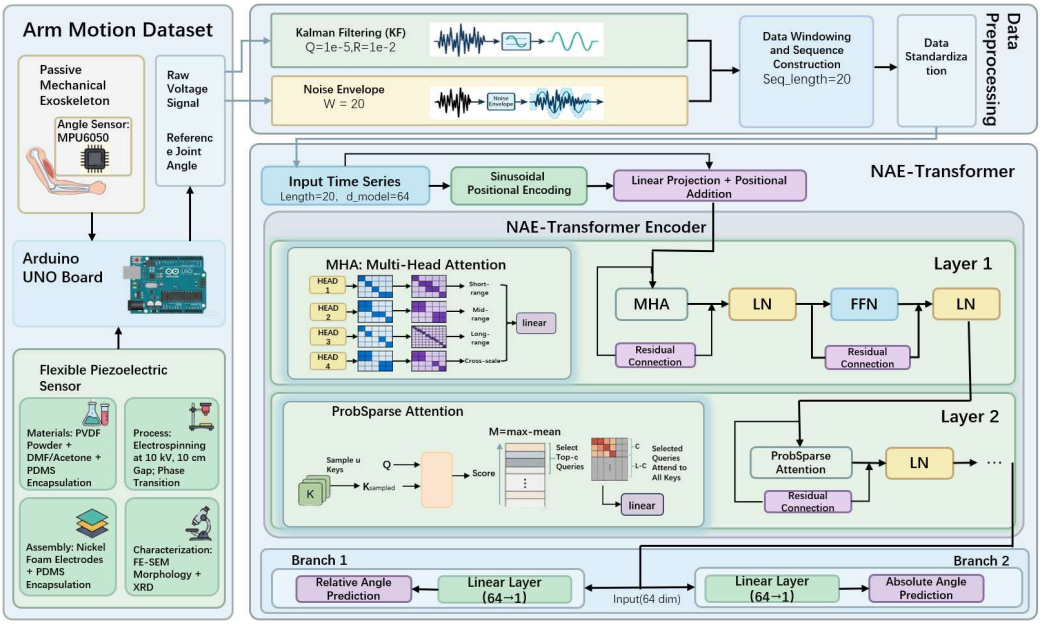


Figure 2. Overall architecture of the proposed NAE-Transformer framework for wearable joint angle prediction.

Feature Embedding and Hybrid Sparse Attention Encoder

For an input sequence $X \in \mathbb{R}^{T\times 2}$, a linear embedding layer and positional encoding map the input into a d_{model}-dimensional representation

$$\tilde{Z} = XW_e + b_e + PE, \qquad \tilde{Z} \in \mathbb{R}^{T\times d_{\text{model}}}, \tag{7}$$

where $d_{\text{model}} = 64$. The encoder contains a standard multi-head self-attention layer followed by a ProbSparse attention layer

$$H = \text{Encoder}_{\text{ProbSparse}}(\text{Encoder}_{\text{MHA}}(\tilde{Z})). \tag{8}$$

Standard self-attention is computed as

$$\text{Attention}(Q,K,V) = \text{Softmax}\left(\frac{QK^T}{\sqrt{d_k}}\right)V, \tag{9}$$

where Q, K, and V are generated from the encoder input. In the higher encoder layer, ProbSparse attention selects queries with larger sparsity scores,

$$M(q_i,K) = \max_j\left(\frac{q_i k_j^T}{\sqrt{d_k}}\right) - \frac{1}{L_K}\sum_{j=1}^{L_K}\left(\frac{q_i k_j^T}{\sqrt{d_k}}\right), \tag{10}$$

thereby preserving dominant dependency relationships while reducing redundant attention computation. In this study, the term "Efficient" refers specifically to the reduction of redundant attention interactions within the proposed dual-representation Transformer framework.

Dual-Output Prediction and Optimization Objective

Based on the shared encoded feature h_t, the model predicts the relative and absolute angles as

$$\hat{y}_t^{\text{rel}} = W_r h_t + b_r, \qquad \hat{y}_t^{\text{abs}} = W_a h_t + b_a. \tag{11}$$

The model is trained using a joint mean squared error loss

$$L = \frac{1}{MT}\sum_{m=1}^{M}\sum_{t=1}^{T}\left[\left(y_{m,t}^{\text{rel}} - \hat{y}_{m,t}^{\text{rel}}\right)^2 + \left(y_{m,t}^{\text{abs}} - \hat{y}_{m,t}^{\text{abs}}\right)^2\right]. \tag{12}$$

This dual-output design jointly constrains local angular variation errors and global angle prediction errors.

Experimental Validation

Sensor Fabrication, Data Acquisition, and Implementation Details

The flexible piezoelectric sensor was fabricated using PVDF (polyvinylidene fluoride) as the piezoelectric matrix. The PVDF powder was dissolved in a DMF (N,N-dimethylformamide)/acetone mixed solvent at a volume ratio of 6:4. PDMS (polydimethylsiloxane) was used as the encapsulation material, with a base-to-curing-agent mass ratio of 10:1. PVDF nanofiber films were prepared by electrospinning to promote molecular chain orientation and the $\alpha \rightarrow \beta$ phase transition. Specifically, 1.208 g of PVDF powder was added to 10 mL of the DMF/acetone mixed solvent to prepare a 12% PVDF solution, which was magnetically stirred for 12 h until fully dissolved. Electrospinning was performed using a positive voltage of 10 kV, a negative voltage of -2 kV, a syringe feeding rate of 1 mL/h, a needle-to-collector distance of 10 cm, a collector roller speed of 140 rad/min, an environmental temperature of 60 °C, humidity below 20%, and a spinning duration of at least 8 h. FE-SEM (field-emission scanning electron microscopy) and XRD (X-ray diffraction) characterization showed that the obtained fibers formed a continuous network structure and exhibited a β-phase characteristic peak at approximately 20.4°, indicating piezoelectric activity in the fabricated PVDF nanofiber film. The sensor fabrication process, material characterization, sensor prototype, and wearable experimental setup are shown in Fig. 3.

The assembled sensor consisted of an electrode layer, a core sensing structure, and a flexible encapsulation layer. Nickel foam was used as the electrode and connected to Dupont wires, with mechanical pressing used to obtain stable conduction. The PVDF nanofiber film was placed between two electrodes to maintain insulation and ensure sufficient contact with the sensing layer. The core structure was then placed in a mold and encapsulated with PDMS. After curing at 65 °C for 60 min in a drying oven, the flexible piezoelectric strain sensor was obtained.

Experimental data were collected using the flexible piezoelectric sensing system described above. The piezoelectric output was acquired with an Arduino UNO board at a sampling frequency of 100 Hz and an analog-to-digital conversion range of

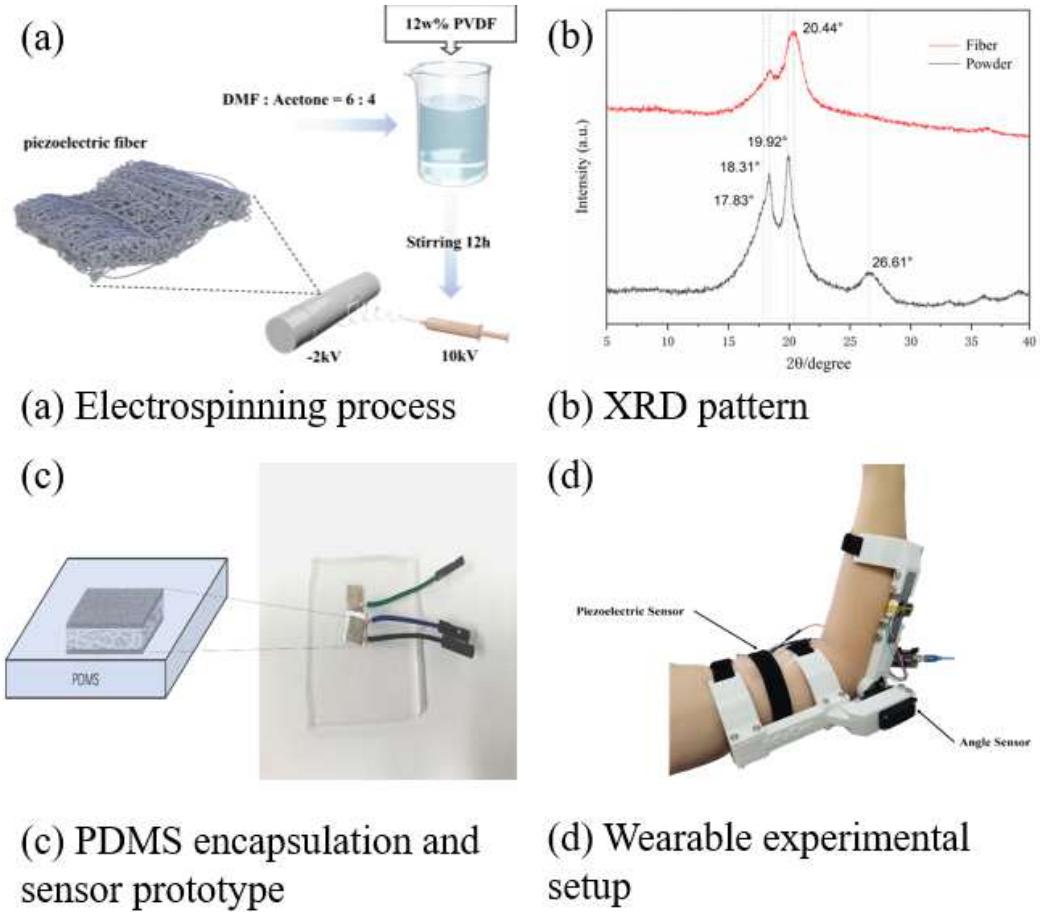


Figure 3. Fabrication, characterization, and experimental setup of the flexible piezoelectric sensor: (a) electrospinning process of the PVDF nanofiber film, (b) XRD pattern of PVDF powder and electrospun PVDF fibers, (c) PDMS-encapsulated sensor structure and prototype, and (d) wearable experimental setup with the passive mechanical exoskeleton and piezoelectric sensor.

0–1023. During each trial, the flexible piezoelectric sensor was attached to the biceps brachii region, and the corresponding elbow angle was recorded using an angle sensor mounted on a passive mechanical exoskeleton. Six participants took part in the experiment and performed elbow flexion at a natural rhythm over an approximate range of 0–100°.

The study and the use of the anonymized experimental data were reviewed and approved by the Zhengzhou University Life Science Ethics Review Committee (approval No. ZZUIRB-2026-173). All methods were carried out in accordance with relevant guidelines and regulations and with the Declaration of Helsinki. Written informed consent was obtained from all participants. The experiment was non-invasive and involved only wearable sensor-based elbow-motion data acquisition. No personally identifiable information was used in the analysis.

The piezoelectric voltage signal and joint angle sequence were collected synchronously, and the angle sensor output was used as the supervised reference label for learning the mapping between piezoelectric signal and joint angle.

The collected data were stored as time-series records, with the piezoelectric signal used as the model input and the joint angle used as the prediction target. The segment from index 2000 to 12000 was selected as the valid sample interval. This valid time-series segment was divided into training and validation sets at a ratio of 8:2 in chronological order. Sliding-window samples were then constructed within each data partition, with each sample containing 20 consecutive time steps. No sliding window was constructed across the boundary between the training and validation segments. To improve training stability, input features and labels were standardized using statistics calculated from the training data.

All experiments were implemented in PyTorch. The Adam optimizer was used with an initial learning rate of 0.001, a batch size of 32, and a maximum of 100 training epochs. During training, the mean squared error loss was used to jointly optimize relative and absolute angle predictions, and a learning-rate scheduling strategy was applied to improve convergence stability. The NAE-Transformer used an input feature dimension of 2, an embedding dimension of 64, four attention heads, two encoder layers, a feedforward hidden dimension of 256, and a dropout rate of 0.1. The first encoder layer used standard multi-head self-attention, whereas the second encoder layer used ProbSparse attention.

Comparison With Baseline Models

LSTM, Transformer, Informer, and their Kalman-filter-enhanced variants were used as baseline models. LSTM represented recurrent neural network modeling of piezoelectric time-series signals. Transformer was used to assess standard self-attention for global temporal dependency modeling. Informer, which uses ProbSparse attention for long-sequence forecasting, was included to compare sparse-attention-based modeling in this task. The corresponding KF-LSTM, KF-Transformer, and KF-Informer models applied Kalman filtering at the input stage to evaluate the influence of signal smoothing. All models used the same data partitioning strategy, training protocol, and evaluation metrics.

Quantitative Performance Evaluation

Model performance was evaluated using Avg. MSE (average mean squared error), $\mathrm{MSE}_{\mathrm{rel}}$ (relative angle mean squared error), $\mathrm{MSE}_{\mathrm{abs}}$ (absolute angle mean squared error), and R^2 (coefficient of determination). The quantitative results are summarized in Table 1.

Table 1. Quantitative Comparison of Different Models in the Joint Angle Prediction Task

Model	Avg. MSE	$\mathrm{MSE}_{\mathrm{rel}}$	$\mathrm{MSE}_{\mathrm{abs}}$	Avg. R^2	R^2_{rel}	R^2_{abs}	Training Time (min)
LSTM	10.1852	0.1212	20.2492	0.9108	0.8547	0.9669	0.96
KF-LSTM	5.6569	0.0130	11.3008	0.9607	0.9598	0.9617	0.97
Transformer	11.8951	0.1896	23.6006	0.8637	0.7649	0.9624	1.90
KF-Transformer	5.5016	0.0145	10.9888	0.9593	0.9538	0.9649	1.90
Informer	40.0598	0.3516	79.7679	0.7148	0.5574	0.8722	2.26
KF-Informer	17.6971	0.0513	35.3429	0.8580	0.8321	0.8838	2.23
NAE-Transformer	3.4957	0.0077	6.9837	0.9762	0.9750	0.9774	3.08

Table 1 summarizes the quantitative comparison. Without Kalman filtering, the Avg. MSE values of LSTM, Transformer, and Informer were 10.1852, 11.8951, and 40.0598, respectively. These results indicate that random noise and local fluctuations in the raw piezoelectric signal reduce the stability of temporal feature learning. After Kalman filtering, the Avg. MSE values of KF-LSTM, KF-Transformer, and KF-Informer decreased to 5.6569, 5.5016, and 17.6971, respectively, showing that signal smoothing improves the input quality for different model families.

NAE-Transformer obtained the lowest Avg. MSE (3.4957) and the highest Avg. R^2 (0.9762) among the compared models. Relative to KF-Transformer, its Avg. MSE decreased from 5.5016 to 3.4957, suggesting that the noise-envelope feature provides complementary local fluctuation information beyond the filtered trend signal. NAE-Transformer also achieved the lowest $\mathrm{MSE}_{\mathrm{rel}}$ and $\mathrm{MSE}_{\mathrm{abs}}$, indicating improvements in both overall angle prediction and local angular variation estimation.

Taken together, these results indicate that the noise-aware dual-representation input provides both smoothed trend information and local fluctuation information, while the hybrid sparse attention encoder supports temporal dependency modeling. This

combination reduced prediction error and improved goodness of fit under noisy flexible piezoelectric sensing conditions.

Ablation Study

Ablation experiments were conducted to assess the contribution of the main components of NAE-Transformer. Three variants were evaluated by removing Kalman filtering, removing the noise-envelope feature, or replacing ProbSparse attention with standard self-attention. The results are shown in Table 2.

Table 2. Ablation Study of the Proposed NAE-Transformer

Model	Avg. MSE	MSE_{rel}	MSE_{abs}	Avg. R^2	R^2_{rel}	R^2_{abs}	Training Time (min)
NAE-Transformer (Full)	3.4957	0.0077	6.9837	0.9762	0.9750	0.9774	3.08
w/o KF	10.5467	0.0271	21.0663	0.9219	0.9120	0.9319	3.27
w/o Noise Envelope	5.5672	0.0162	11.1182	0.9557	0.9474	0.9641	2.74
w/o ProbSparse	4.0048	0.0099	7.9996	0.9709	0.9677	0.9741	3.23

Table 2 reports the ablation results. The full model achieved an Avg. MSE of 3.4957. Removing Kalman filtering increased the Avg. MSE to 10.5467, which was the largest degradation among the ablation settings. This result indicates that the smoothed trend input is important for modeling noisy piezoelectric signals.

Removing the noise-envelope feature increased the Avg. MSE to 5.5672, with higher MSE_{rel} and MSE_{abs} than the full model. This result suggests that the local fluctuation information extracted by the sliding-window standard deviation contributes to angle prediction, particularly for characterizing dynamic changes between adjacent time steps.

Replacing ProbSparse attention with standard self-attention increased the Avg. MSE to 4.0048 and increased the training time from 3.08 min to 3.23 min. Relative to this variant, the full NAE-Transformer reduced both training time and prediction error. This result suggests that ProbSparse attention reduces redundant attention interactions within the dual-representation framework while maintaining prediction accuracy. Accordingly, "Efficient" in NAE-Transformer refers to attention interaction reduction within the same model framework rather than shorter training time relative to all baseline models.

Overall, the complete NAE-Transformer achieved the best performance across the reported metrics. The ablation results indicate that the Kalman-smoothed signal, noise-envelope feature, and hybrid sparse attention encoder contribute to trend extraction, local fluctuation representation, and temporal dependency modeling, respectively.

Training Convergence Analysis

Training stability was evaluated by comparing the training and validation loss curves of LSTM, Transformer, Informer, their Kalman-filtered variants, and NAE-Transformer. Fig. 4 shows the corresponding loss curves.

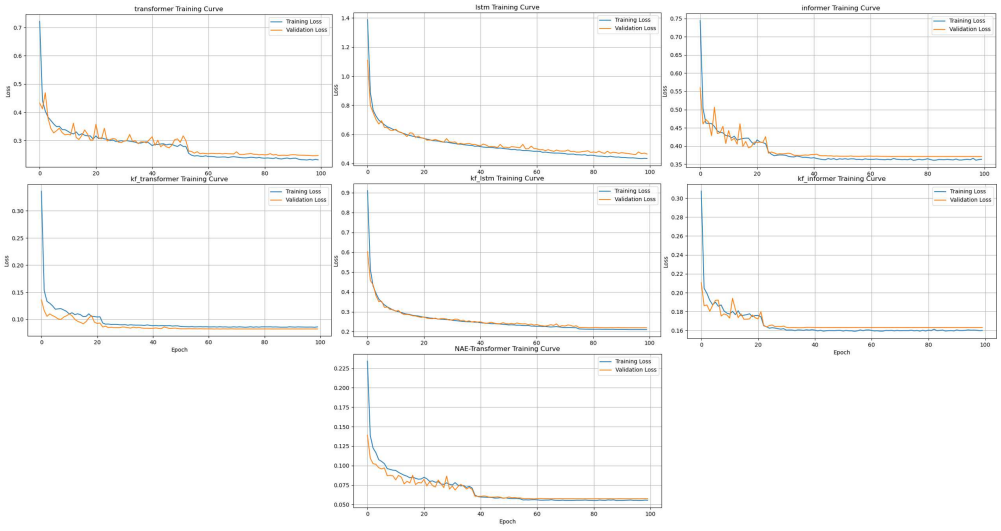


Figure 4. Training and validation loss curves of different models.

The models without filtering showed slower loss reduction during early training, and their validation losses exhibited noticeable fluctuations. This behavior suggests that random noise in the raw piezoelectric signal affected model optimization. After Kalman filtering was introduced, the loss curves became smoother and converged more rapidly.

The validation loss of NAE-Transformer showed mild fluctuations in the early training stage, likely because of its larger model capacity and the coordination of dual-representation features. In the later training stage, however, NAE-Transformer reached a lower validation loss than the standard Transformer and KF-Transformer. This suggests that the dual-representation

input provides complementary signal descriptions and that the hybrid sparse attention encoder supports more stable temporal feature learning.

Angle Prediction Visualization

Absolute Angle Prediction

Absolute angle predictions were visually compared to assess model behavior over time. To maintain readability, four representative models were selected: LSTM, Transformer, KF-Transformer, and NAE-Transformer. These models represent recurrent modeling, standard attention modeling, filtering-enhanced attention modeling, and the proposed framework, respectively. Fig. 5 shows the absolute angle prediction results.

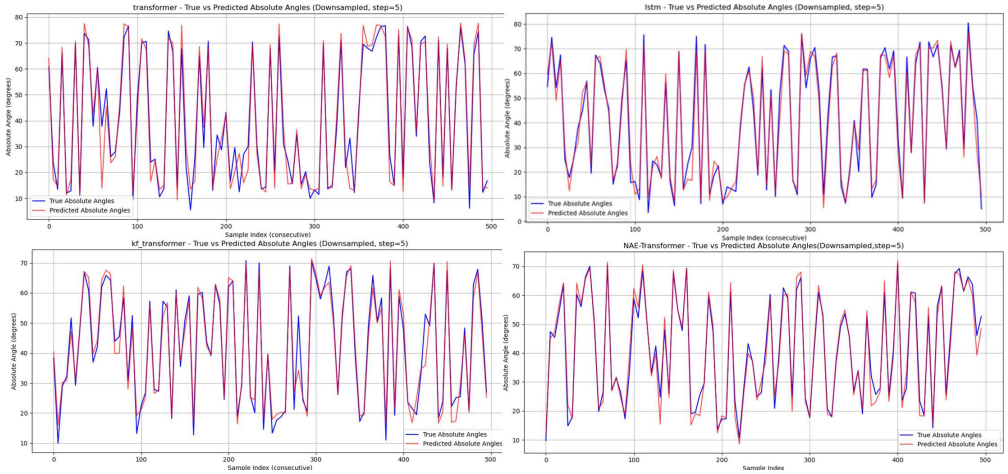


Figure 5. Absolute angle prediction results of representative models, including LSTM, Transformer, KF-Transformer, and NAE-Transformer.

The prediction curves show that LSTM and Transformer deviated from the reference signal near several peaks and valleys, suggesting that raw-signal noise affects the fitting of large-amplitude angle variations. After Kalman filtering, KF-Transformer showed better consistency with the reference angle. NAE-Transformer provided more stable tracking in several peak, valley, and transition regions, with high overall agreement with the reference angle. Because the absolute angle sequence has a clear global trend, the visual difference between KF-Transformer and NAE-Transformer is moderate; therefore, these curves should be interpreted together with the quantitative metrics and the relative angle prediction results.

Relative Angle Prediction

Relative angle prediction is more sensitive to local changes during joint motion and therefore imposes higher requirements on temporal modeling. The same four representative models were compared. Fig. 6 shows the relative angle prediction results.

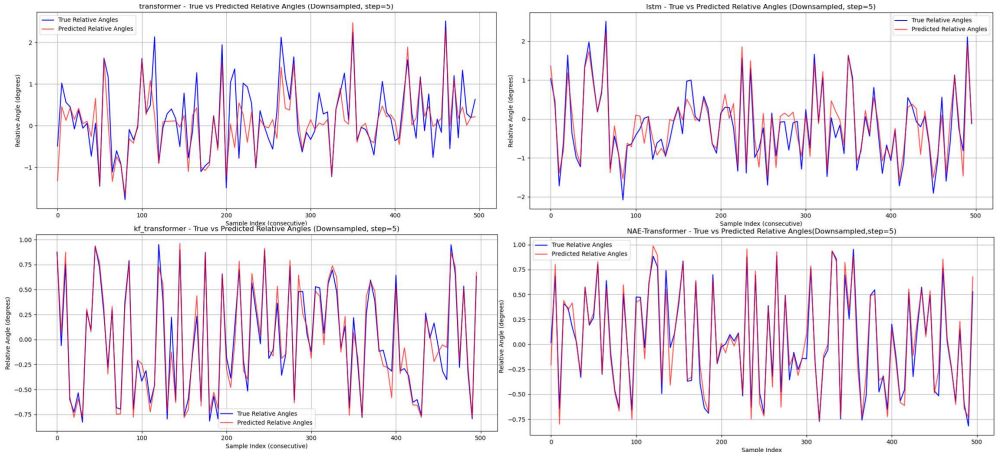
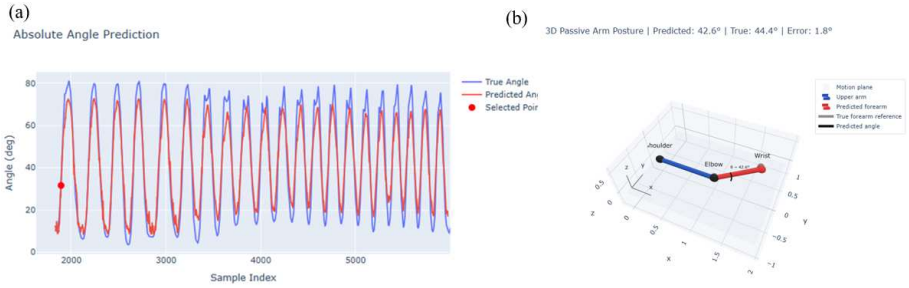


Figure 6. Relative angle prediction results of representative models, including LSTM, Transformer, KF-Transformer, and NAE-Transformer.

In the relative angle curves, LSTM and Transformer without filtering showed larger fluctuations during intervals with rapid local changes. KF-Transformer produced smoother predictions overall, but deviations remained at some local change points. NAE-Transformer more closely followed the direction of the reference relative angle at most time steps, suggesting that the noise-envelope feature provides local dynamic information that improves relative angle prediction.

Three-Dimensional Motion Reconstruction Validation

The usability of the predicted angles was further examined through motion reconstruction. The elbow angles predicted by NAE-Transformer were input into a simplified upper-limb kinematic model, and the forearm posture was updated accordingly. This reconstruction experiment was not used for model training and served only to assess whether the predicted angles could support posture reconstruction.



(a) Selected point on the absolute angle prediction curve

(b) 3D passive arm posture reconstructed from the predicted angle

Figure 7. Three-dimensional motion reconstruction validation: (a) selected point on the absolute angle prediction curve and (b) corresponding passive arm posture reconstructed from the predicted elbow joint angle.

Fig. 7 shows the three-dimensional reconstruction corresponding to a selected point on the absolute angle prediction curve. The forearm posture reconstructed from the NAE-Transformer predictions was generally consistent with the reference posture. During large angle variations, the predicted posture maintained a direction of change close to the reference motion trend. This result suggests that the model output can support simplified upper-limb motion reconstruction in addition to providing low numerical error.

Conclusion

This study presented an NAE-Transformer model for joint angle prediction from flexible piezoelectric signals. By combining a Kalman-smoothed trend signal, a sliding-window noise envelope, and a hybrid sparse attention encoder, the model improved absolute and relative angle prediction compared with LSTM, Transformer, Informer, and their Kalman-filter-enhanced variants. The ablation results further supported the contributions of trend smoothing, local fluctuation representation, and ProbSparse attention. Future work will extend the experiments to larger subject groups and cross-scenario settings, and will examine embedded deployment in wearable systems.

Data availability

The data supporting the findings of this study are available from the corresponding author upon reasonable request, subject to participant privacy and institutional restrictions.

Funding

The authors received no funding for this work.

Acknowledgements

The authors thank the participants who took part in the data acquisition experiments.

Author contributions statement

Z.L. conceived the study, developed the prediction model, performed data analysis, and drafted the manuscript. Y.T. contributed to sensor fabrication, characterization, and experimental preparation. K.S. contributed to data collection, experimental validation, and result organization. Z.C. supervised sensor fabrication and materials-related analysis and revised the manuscript. S.C. contributed to participant-related experimental guidance and manuscript revision. R.W. supervised the research, guided the modeling and experimental design, and revised the manuscript. All authors reviewed and approved the final manuscript.

Additional information

Competing interests: The authors declare no competing interests.

ORCID: Zongyuan Li, 0000-0001-9743-4515; Yanzhi Tang, 0009-0003-5919-2043; Kexin Su, 0009-0000-9176-6340; Zhimin Chen, 0000-0002-6978-1330; Suyan Chen, 0009-0004-1863-5554; Ruijuan Wang, 0000-0001-9999-9990.

References

1. J. Coker, H. Chen, M. C. Schall Jr., S. Gallagher, and M. Zabala, "EMG and joint angle-based machine learning to predict future joint angles at the knee," *Sensors*, vol. 21, no. 11, Art. no. 3622, 2021, doi: 10.3390/s21113622.
2. O. N. Beck, M. K. Shepherd, R. Rastogi, G. Martino, L. H. Ting, and G. S. Sawicki, "Exoskeletons need to react faster than physiological responses to improve standing balance," *Science Robotics*, vol. 8, no. 75, Art. no. eadf1080, 2023, doi: 10.1126/scirobotics.adf1080.
3. O. D. Lara and M. A. Labrador, "A survey on human activity recognition using wearable sensors," *IEEE Communications Surveys & Tutorials*, vol. 15, no. 3, pp. 1192–1209, 2013, doi: 10.1109/SURV.2012.110112.00192.
4. F. Demrozi, G. Pravadelli, A. Bihorac, and P. Rashidi, "Human activity recognition using inertial, physiological and environmental sensors: A comprehensive survey," *IEEE Access*, vol. 8, pp. 210816–210836, 2020, doi: 10.1109/ACCESS.2020.3037715.
5. Y. Weizman *et al.*, "Wearable IMU sensors in people living with spasticity: A systematic review," *Sensors*, vol. 22, no. 5, Art. no. 1791, 2022, doi: 10.3390/s22051791.
6. H. Dejnabadi, B. M. Jolles, and K. Aminian, "A new approach to accurate measurement of uniaxial joint angles based on a combination of accelerometers and gyroscopes," *IEEE Transactions on Biomedical Engineering*, vol. 52, no. 8, pp. 1478–1484, 2005, doi: 10.1109/TBME.2005.851475.
7. P. Picerno, "25 years of lower limb joint kinematics by using inertial and magnetic sensors: A review of methodological approaches," *Gait & Posture*, vol. 51, pp. 239–246, 2017, doi: 10.1016/j.gaitpost.2016.11.008.
8. A. M. Sabatini, "Quaternion-based extended Kalman filter for determining orientation by inertial and magnetic sensing," *IEEE Transactions on Biomedical Engineering*, vol. 53, no. 7, pp. 1346–1356, 2006, doi: 10.1109/TBME.2006.875664.
9. L. Pacher, C. Chatellier, R. Vauzelle, and L. Fradet, "Sensor-to-segment calibration methodologies for lower-body kinematic analysis with inertial sensors: A systematic review," *Sensors*, vol. 20, no. 11, Art. no. 3322, 2020, doi: 10.3390/s20113322.
10. D. Xiong, D. Zhang, X. Zhao, and Y. Zhao, "Deep learning for EMG-based human-machine interaction: A review," *IEEE/CAA Journal of Automatica Sinica*, vol. 8, no. 3, pp. 512–533, 2021, doi: 10.1109/JAS.2021.1003865.
11. M. Amjadi, K.-U. Kyung, I. Park, and M. Sitti, "Stretchable, skin-mountable, and wearable strain sensors and their potential applications: A review," *Advanced Functional Materials*, vol. 26, no. 11, pp. 1678–1698, 2016, doi: 10.1002/adfm.201504755.
12. T. Q. Trung and N.-E. Lee, "Flexible and stretchable physical sensor integrated platforms for wearable human-activity monitoring and personal healthcare," *Advanced Materials*, vol. 28, no. 22, pp. 4338–4372, 2016, doi: 10.1002/adma.201504244.
13. C. Dagdeviren *et al.*, "Conformal piezoelectric energy harvesting and storage from motions of the heart, lung, and diaphragm," *Proceedings of the National Academy of Sciences of the United States of America*, vol. 111, no. 5, pp. 1927–1932, 2014, doi: 10.1073/pnas.1317233111.
14. H. Kim *et al.*, "Estimation of hand motion from piezoelectric soft sensor data using deep learning," *Applied Sciences*, vol. 10, no. 6, Art. no. 2194, 2020, doi: 10.3390/app10062194.
15. J. Chang, J. Li, J. Ye, B. Zhang, J. Chen, Y. Xia, J. Lei, T. Carlson, R. Loureiro, A. M. Korsunsky, J.-C. Tan, and H. Zhao, "AI-enabled piezoelectric wearable for joint torque monitoring," *Nano-Micro Letters*, vol. 17, Art. no. 247, 2025, doi: 10.1007/s40820-025-01753-w.
16. X. Cao, Y. Xiong, J. Sun, X. Zhu, Q. Sun, and Z. L. Wang, "Piezoelectric nanogenerators derived self-powered sensors for multifunctional applications and artificial intelligence," *Advanced Functional Materials*, vol. 31, no. 33, Art. no. 2102983, 2021, doi: 10.1002/adfm.202102983.
17. Y. Chen, X. Zhang, and C. Lu, "Flexible piezoelectric materials and strain sensors for wearable electronics and artificial intelligence applications," *Chemical Science*, vol. 15, no. 40, pp. 16436–16466, 2024, doi: 10.1039/D4SC05166A.
18. J. Wu, Z. Mo, X. Gao, W. Xin, W. Shi, and J. Park, "Artificial intelligence assisted wearable flexible sensors for sports: research progress in technology integration and application," *International Journal of Smart and Nano Materials*, vol. 16, no. 3, pp. 510–548, 2025, doi: 10.1080/19475411.2025.2519582.
19. D. Hollinger, M. C. Schall Jr., H. Chen, and M. Zabala, "The effect of sensor feature inputs on joint angle prediction across simple movements," *Sensors*, vol. 24, no. 11, Art. no. 3657, 2024, doi: 10.3390/s24113657.
20. J. Wang, Y. Chen, S. Hao, X. Peng, and L. Hu, "Deep learning for sensor-based activity recognition: A survey," *Pattern Recognition Letters*, vol. 119, pp. 3–11, 2019, doi: 10.1016/j.patrec.2018.02.010.
21. F. J. Ordonez and D. Roggen, "Deep convolutional and LSTM recurrent neural networks for multimodal wearable activity recognition," *Sensors*, vol. 16, no. 1, Art. no. 115, 2016, doi: 10.3390/s16010115.
22. K. Chen, D. Zhang, L. Yao, B. Guo, Z. Yu, and Y. Liu, "Deep learning for sensor-based human activity recognition: Overview, challenges, and opportunities," *ACM Computing Surveys*, vol. 54, no. 4, Art. no. 77, 2021, doi: 10.1145/3447744.
23. A. Murad and J.-Y. Pyun, "Deep recurrent neural networks for human activity recognition," *Sensors*, vol. 17, no. 11, Art. no. 2556, 2017, doi: 10.3390/s17112556.
24. J. Sung, S. Han, H. Park, H.-M. Cho, S. Hwang, J. W. Park, and I. Youn, "Prediction of lower extremity multi-joint angles during overground walking by using a single IMU with a low frequency based on an LSTM recurrent neural network," *Sensors*, vol. 22, no. 1, Art. no. 53, 2022, doi: 10.3390/s22010053.
25. M. Abdelhady, D. L. Damiano, and T. C. Bulea, "Knee angle estimation from surface EMG during walking using attention-based deep recurrent neural networks: Feasibility and initial demonstration in cerebral palsy," *Sensors*, vol. 24, no. 13, Art. no. 4217, 2024, doi: 10.3390/s24134217.
26. A. Vaswani *et al.*, "Attention is all you need," in *Advances in Neural Information Processing Systems*, vol. 30, 2017.
27. H. Zhou, S. Zhang, J. Peng, S. Zhang, J. Li, H. Xiong, and W. Zhang, "Informer: Beyond efficient Transformer for long sequence time-series forecasting," in *Proc. AAAI Conference on Artificial Intelligence*, vol. 35, no. 12, pp. 11106–11115, 2021, doi: 10.1609/aaai.v35i12.17325.
28. H. Wu, J. Xu, J. Wang, and M. Long, "Autoformer: Decomposition Transformers with auto-correlation for long-term series forecasting," in *Advances in Neural Information Processing Systems*, vol. 34, pp. 22419–22430, 2021.
29. E. Aksan, M. Kaufmann, P. Cao, and O. Hilliges, "A spatio-temporal Transformer for 3D human motion prediction," in *Proc. International Conference on 3D Vision (3DV)*, 2021, pp. 565–574, doi: 10.1109/3DV53792.2021.00066.

30. R. E. Kalman, "A new approach to linear filtering and prediction problems," *Journal of Basic Engineering*, vol. 82, no. 1, pp. 35–45, 1960, doi: 10.1115/1.3662552.

31. S. J. Julier and J. K. Uhlmann, "Unscented filtering and nonlinear estimation," *Proceedings of the IEEE*, vol. 92, no. 3, pp. 401–422, 2004, doi: 10.1109/JPROC.2003.823141.

32. G. Welch and G. Bishop, "An introduction to the Kalman filter," University of North Carolina at Chapel Hill, Chapel Hill, NC, USA, Tech. Rep. TR 95-041, 2006.